Application of a κ-ϵ turbulence model to the prediction of noise for simple and coaxial free jets

W. Béchara,[a] P. Lafon, and C. Bailly
Electricité de France, DER-AMV, 1 Av. du Général-de-Gaulle, 92141 Clamart Cedex, France

S. M. Candel
Ecole Centrale Paris, Grande Voie des Vignes, 92295 Châtenay-Malabry Cedex, France

(Received 7 May 1992; revised 25 August 1994; accepted 21 January 1995)

A numerical solution of a κ-ϵ turbulence model is used to provide local and statistical properties throughout simple and coaxial round jets. These are inserted into predictive formulas for jet noise based on Lighthill's theory: Ribner's formalism postulates locally isotropic turbulence superposed on mean flow; Goldstein and Rosenbaum's formalism generalizes this to accommodate the more realistic assumption of axisymmetry. Numerical jet noise predictions via the Ribner/κ-ϵ model (designated R_a) and the Goldstein/κ-ϵ model (designated G_a), and some variants, are compared with experiment. Only a single empirical factor is used. The G_a model, with its threefold longer axial scale, shows closer agreement with experiment than the R_a model. The predictive capacity of the G_a model is demonstrated by further calculations for coaxial jets. The results confirm the experimental observation of a minimum of acoustic radiation when the outer flow has 0.4 the velocity of the inner flow. An advantage of the κ-ϵ method is that it yields information on the spatial and spectral distribution of the acoustic sources.

PACS numbers: 43.28.Ra, 43.50.Nm

INTRODUCTION

Current formulations of the generation of aerodynamic noise by turbulence all require statistical information with regard to the turbulent flow field. The most popular of these, based on the general theory for flow noise of Lighthill,[1,2] are the specialized formulations for jet noise of Proudman,[3] Lilley,[4] Ribner,[5,6] Pao,[7] and Goldstein *et al.*[8] The specialized formulations provide a framework for estimating the source terms (via correlations) required by the general theory. Under certain simplifying assumptions, all specialized theories lead to analytical expressions which allow a prediction of the noise radiation from a fairly small number of local turbulent quantities. To estimate these quantities, the tendency has been to use various similarity arguments which allow a proper description of the turbulence characteristics of free jets. However, these similarity arguments may not be applicable for more complex ejection configurations due to the modification of the turbulent flow characteristics. For example, the similarity approach has difficulties in handling coaxial jets. A more general approach, using second-order closure turbulence theory was explored by Bilanin *et al.*[9] In this approach, an early model of Ribner[5] for noise generation was coupled with the predictions of a κ-l turbulence model to estimate the noise radiated from standard and swirling jets. Looking back at this contribution, one may say that it was not fully successful because the noise model was too crude and as a consequence the scaling factor was not constant.

In the present paper, we follow a similar strategy, but we use more advanced versions of noise formulations (Ribner,[6] Goldstein *et al.*[8]) in association with Reynolds average Navier-Stokes computations based on a κ-ϵ turbulence model. Our purpose is to devise a predictive package which provides the main acoustic characteristics.

This paper is organized as follows:

In Sec. I, the noise generation models due to Ribner[6] and its generalization by Goldstein *et al.*[8] are reviewed and the modifications and assumptions required to utilize predictions from the κ-ϵ model are provided. In Sec. II, computations of the acoustic properties are given for a simple cold round jet. These computations are compared to the experimental data of Lush.[10] In Sec. III, we check the generality of the present formulation, by carrying out a parametric study of the noise radiation from two coaxial jets. The effect of velocity ratio is specifically considered and the results are compared with the experimental data of Juvé *et al.*[11]

I. THEORETICAL BACKGROUND

In this section, we briefly review Lighthill's theory of noise generated by turbulent flows and its application to the case of turbulent jets. We also present the theoretical models of Ribner[6] and Goldstein *et al.*[8] We will focus on assumptions utilized and on adaptations required by these descriptions.

A. Application of Lighthill theory

Lighthill[1,2] has shown that the density fluctuations detected at a point **x** in the far field and originated from a localized turbulent region (V) is given by

[a]Present address: Centre de Recherche Claude Delorme de l'Air Liquide-BP126 78350 Les Loges en Josas-France.

 0001-4966/95/97(6)/3518/14/$6.00

$$\rho(\mathbf{x},t)-\rho_0=\frac{x_i x_j}{4\pi c_0^4 x^3}\int_V \frac{\partial^2}{\partial t^2} T_{ij}\left(\mathbf{y},t-\frac{|\mathbf{x}-\mathbf{y}|}{c_0}\right)d\mathbf{y},$$

$$T_{ij}=\rho u_i u_j+[(p-p_0)-c_0^2(\rho-\rho_0)]\delta_{ij}+\tau_{ij}, \tag{1}$$

where T_{ij} is the instantaneous Lighthill tensor, τ_{ij} the viscous stresses tensor, p and ρ are the local pressure and density, p_0, ρ_0, and c_0 the ambient pressure, density, and speed of sound, u_i is the velocity, t is the time variable, and $\delta_{ij}=0$ or 1 as $i\neq j$ or $i=j$; $i,j=1,2,3$, and repeated indices are summed over. The origin of the x,y coordinates is taken within the flow. In isothermal turbulent flows at high Reynolds number, the source term T_{ij} is dominated by the intensity of turbulence $\rho u_i u_j$. If the Mach number is not too large, then T_{ij} can be approximated by $\rho_0 u_i u_j$. In such flows where it is reasonable to suppose that T_{ij} is a stationary random function of time, one can define the density autocorrelation function by

$$C_{\rho\rho}(\mathbf{x},\tau)=\frac{\overline{[\rho(\mathbf{x},t+\tau)-\rho_0][\rho(\mathbf{x},t)-\rho_0]}}{\rho_0 c_0^{-3}}. \tag{2}$$

It follows from Eq. (1) that this function is related to the source term by

$$C_{\rho\rho}(\mathbf{x},\tau)$$
$$=\frac{\rho_0 x_i x_j x_k x_l}{16\pi^2 c_0^5 x^6}$$
$$\times\int\int_V \overline{\frac{\partial^2}{\partial t^2}u_i' u_j'(\mathbf{y}',t')\frac{\partial^2}{\partial t^2}u_k'' u_l''(\mathbf{y}',t'')}d\mathbf{y}'\,d\mathbf{y}'', \tag{3}$$

where $t'=t-|\mathbf{x}-\mathbf{y}'|/c_0$; $t''=t+\tau-|\mathbf{x}-\mathbf{y}''|/c_0$, $\mathbf{y}'$ and $\mathbf{y}''$ are two running points in the source domain (V). This domain (V) is identified to the one occupied by the jet flow. Ffowcs Williams[12] shows that Eq. (3) can be cast in the following form:

$$C_{\rho\rho}(\mathbf{x},\tau)=\rho_0\frac{x_i x_j x_k x_l}{16\pi^2 c_0^5 x^6}\int\int_V \frac{\partial^4}{\partial\tau^4}\mathrm{R}_{ijkl}\left(\mathbf{y}',\boldsymbol{\eta},\tau+\frac{\boldsymbol{\eta}\cdot\mathbf{x}}{c_0 x}\right)$$
$$\times\,d\mathbf{y}'\,d\boldsymbol{\eta},$$

$$\mathrm{R}_{ijkl}(\mathbf{y}',\boldsymbol{\eta},\tau)=\overline{u_i' u_j'(\mathbf{y}',t)u_k'' u_l''(\mathbf{y}'',t+\tau)}-\mathrm{R}_{ijkl}^0(\mathbf{y}',\boldsymbol{\eta}), \tag{4}$$

where R_{ijkl} represents the two-point time-delayed fourth-order correlation tensor. It is found convenient to introduce an arbitrary time-independent tensor R_{ijkl}^0 which is eventually chosen to simplify further algebraic calculations of the integrand. Equation (4) uses the vector separation $\boldsymbol{\eta}=\mathbf{y}''-\mathbf{y}'$ and the retarded time $\mathbf{x}\,\boldsymbol{\eta}/xc_0$ observed at the point $\mathbf{x}$ for two acoustic waves emitted at the same time at points $\mathbf{y}'$ and $\mathbf{y}''$.

Now, as explained by Lighthill[2] and Ffowcs Williams,[12] one can introduce the moving-axis transformation

$$\boldsymbol{\xi}=\boldsymbol{\eta}-\hat{\imath}U_{1c}\tau \tag{5}$$

(where U_{1c} is the axial eddy convection velocity in the direction of the unit vector $\hat{\imath}$ which is the mean flow direction) into Eq. (4) in order to neglect retarded time effects. Notice that this moving axis transformation is an optional choice to

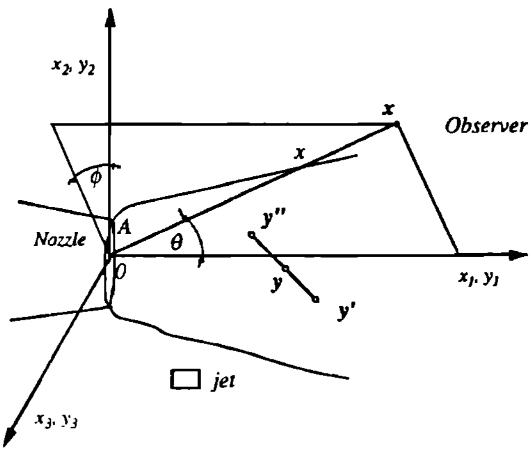

FIG. 1. Turbulent jet flow configuration. (x,θ,ϕ are the spherical coordinates of the point of observation $\mathbf{x}$, D is the diameter of the nozzle and $\mathbf{y}$ is the midpoint of the two source points $\mathbf{y}'$ and $\mathbf{y}''$.)

account for source convection. Alternatively, the nozzle-fixed axes may be retained and source motion allowed for in the form of the R_{ijkl}. Ribner[5] employs the latter and demonstrates the equivalence. Thus upon introducing the moving-frame correlation tensor, $R_{ijkl}(\mathbf{y}',\boldsymbol{\xi},\tau)=\mathrm{R}_{ijkl}(\mathbf{y}',\boldsymbol{\eta},\tau)$, Eq. (4) becomes after eliminating retarded time effects:

$$C_{\rho\rho}(\mathbf{x},\tau')=\frac{\rho_0 x_i x_j x_k x_l}{16\pi^2 c_0^5 x^6}\int\int_V \frac{1}{C^5}$$
$$\times\left(\frac{\partial^4}{\partial\tau^4}\mathbf{R}_{ijkl}(\mathbf{y}',\boldsymbol{\xi},\tau)\right)_{\tau=\tau'/C}d\boldsymbol{\xi}\,d\mathbf{y}', \tag{6}$$

where C is the convection factor $C=1-M_c\cos\theta$; $\cos\theta=x_1/x$, θ is the angle between the direction of mean flow and the direction of observation $\mathbf{x}$ (see Fig. 1), and M_c designates the convection Mach number. Following Ribner[6] we let $C_{\rho\rho}(\mathbf{x}/\mathbf{y}',\tau)$ denote the autocorrelation function at the point $\mathbf{x}$ due to the sound emitted from a unit volume at $\mathbf{y}'$. Then

$$C_{\rho\rho}(\mathbf{x},\tau')=\int_{\mathrm{jet}} C_{\rho\rho}\left(\frac{x}{\mathbf{y}'},\tau'\right)d\mathbf{y}'$$

and

$$C_{\rho\rho}\left(\frac{x}{\mathbf{y}'},\tau'\right)=\frac{\rho_0 x_i x_j x_k x_l}{16\pi^2 c_0^5 x^6}\int_V \frac{1}{C^5}$$
$$\times\left(\frac{\partial^4}{\partial\tau^4}R_{ijkl}(\mathbf{y}',\boldsymbol{\xi},\tau)\right)_{\tau=\tau'/C}d\boldsymbol{\xi}. \tag{7}$$

B. Ribner model

In his two first models, Ribner[5,13] rewrites Eq. (7) in a form inspired from Proudman[3] where $\overline{u_x'^2 u_x''^2}$ governs the acoustic emission in the $\mathbf{x}$ direction (the x index indicates that the velocity is projected in the observation direction). This Proudman form is by far the simpler: The single correlation $\overline{u_x'^2 u_x''^2}$ replaces some 36 correlations $\overline{u_i' u_j' u_k'' u_l''}$. In a later model, Ribner[6] reformulates the model so as to calculate the relative contributions of all the different correlations. The assumptions made are the following:

(A1) The noise pattern of the round jet considered is axisymmetric, so that the autocorrelation function $C_{\rho\rho}$ is independent of ϕ (see Fig. 1).

(A2) The mean flow is nearly parallel and in that case, it is of interest to decompose the instantaneous local velocity as a sum of a parallel mean flow and turbulent fluctuations with zero mean so that

$$u_i(\mathbf{y},t)=U_i(\mathbf{y})\,\delta_{1i}+u_{ti}(\mathbf{y},t). \tag{8}$$

Introducing this decomposition into R_{ijkl} and assuming that the turbulence is locally homogeneous, R_{ijkl} can be written in the form [for $R^0_{ijkl}(\mathbf{y},\boldsymbol{\xi})=0$]:

$$\begin{aligned}R_{ijkl}(\mathbf{y},\boldsymbol{\xi},\tau)=&\overline{u'_{ti}u'_{tj}u''_{tk}u''_{tl}}+U'_1U''_1(\delta_{1i}\delta_{1k}\overline{u'_{tj}u''_{tl}}\\&+\delta_{1j}\delta_{1l}\overline{u'_{ti}u''_{tk}}+\delta_{1j}\delta_{1k}\overline{u'_{ti}u''_{tl}}\\&+\delta_{1i}\delta_{1l}\overline{u'_{tj}u''_{tk}}).\end{aligned} \tag{9}$$

The noise associated with the first term is called "self-noise." It represents the contribution arising from turbulence alone. The other terms represent components due to the interaction between turbulence and mean flow. These contributions form the "shear noise."

(A3) The joint probability of u'_{ti} and u''_{ti} is assumed to be normal, thus it follows that:

$$\begin{aligned}\overline{u'_{ti}u'_{tj}u''_{tk}u''_{tl}}(\mathbf{y},\boldsymbol{\xi},\tau)=&R_{ij}(\mathbf{y},0,0)R_{kl}(\mathbf{y},0,0)\\&+(R_{ik}R_{jl}+R_{il}R_{jk})(\mathbf{y},\boldsymbol{\xi},\tau),\end{aligned} \tag{10}$$

where

$$R_{ij}(\mathbf{y},\boldsymbol{\xi},\tau)=\overline{u'_{ti}u''_{tj}}(\mathbf{y},\boldsymbol{\xi},\tau).$$

(A4) The two-point correlation $R_{ij}(\mathbf{y},\boldsymbol{\xi},\tau)$ is factorable into a space factor and a time factor. If these two parts are assumed to be Gaussian and the turbulence is isotropic, this correlation takes the form:

$$R_{ij}(\mathbf{y},\boldsymbol{\xi},\tau)=R_{ij}(\mathbf{y},\boldsymbol{\xi})\exp(-\omega_f^2\tau^2), \tag{11a}$$

$$R_{ij}(\mathbf{y},\boldsymbol{\xi})=\overline{u^2_{tm}}\left[\left(f+\frac{1}{2}\,\xi f\,\frac{\partial f}{\partial\xi}\right)\delta_{ij}-\frac{1}{2}\,\frac{\partial f}{\partial\xi}\,\frac{\xi_i\xi_j}{\xi}\right], \tag{11b}$$

$$f(\xi)=\exp(-\pi\xi^2/L_1^2), \tag{11c}$$

where f is the longitudinal correlation function, ω_f is a typical angular frequency of the turbulence, L_1 designates the longitudinal integral scale of the turbulence and $\overline{u^2_{tm}}$ represents $\frac{2}{3}$ of the kinetic turbulent energy κ.

(A5) Finally, one has to evaluate the two point function $U'_1(\mathbf{y}')U''_1(\mathbf{y}'')$ in terms of $U_1^2(\mathbf{y})$ where $\mathbf{y}$ is the midpoint of $\mathbf{y}'$ and $\mathbf{y}''$. The modeling proposed by Ribner[6] is a Gaussian expression $U_1^2(\mathbf{y})\exp(-\sigma\pi\xi_2^2/L_1^2)$, where σ is a local coefficient equal to 0.07. However this modeling is not well adapted to real situations. In fact, based upon a given velocity field, we have recalculated the coefficient σ for different points at the axial position $y_1/D=4$ and for four positions in the transverse direction ($y_2/D=0$, 0.5, 1, and 3). The numerical calculations[14] show that σ is not constant, and furthermore we notice a considerable divergence when $y_2/D\geqslant 1$, between the exact and modeled values of $U'_1(\mathbf{y}')U''_1(\mathbf{y}'')$.

To avoid this modeling, we perform a Taylor expansion of $U'_1(\mathbf{y}')U''_1(\mathbf{y}'')$ to the first order around the midpoint $\mathbf{y}$ and obtain

$$\begin{aligned}U'_1(\mathbf{y}')U''_1(\mathbf{y}'')&=U_1\left(\mathbf{y}-\frac{\xi_2}{2}\right)U_1\left(\mathbf{y}+\frac{\xi_2}{2}\right)\\&=U_1^2(\mathbf{y})-\frac{\xi_2^2}{4}\left(\frac{\partial U_1}{\partial y_2}(\mathbf{y})\right)^2.\end{aligned} \tag{12}$$

Inserting all these assumptions into Eq. (7), the expressions of the acoustical directional intensity for the shear and self-noise per unit volume of the jet, are simply obtained from the corresponding autocorrelation function for $\tau=0$:

$$\begin{aligned}I^{\text{Se.N.}}(x,\theta/\mathbf{y})&=C^{\text{Se.N.}}_{\rho\rho}(x,\theta/\mathbf{y},\tau=0)\\&=\frac{3\sqrt{2}\rho_0L_1^3\overline{u^2_{tm}}^2}{4\pi^2c_0^5x^2}\,\omega_f^4\,\frac{D_i^{\text{Se.N.}}}{C^5},\end{aligned} \tag{13}$$

$$\begin{aligned}I^{\text{Sh.N.}}(x,\theta/\mathbf{y})&=C^{\text{Sh.N.}}_{\rho\rho}(x,\theta/\mathbf{y},\tau=0)\\&=\frac{3}{8}\,\frac{\rho_0L_1^5\overline{u^2_{tm}}}{\pi^3c_0^5x^2}\left(\frac{\partial U_1}{\partial y_2}\right)^2\omega_f^4\,\frac{D_i^{\text{Sh.N.}}}{C^5},\end{aligned} \tag{14}$$

where $D_i^{\text{Sh.N.}}=1/2(\cos^2\theta+\cos^4\theta)$ and $D_i^{\text{Se.N.}}=1$ are the intrinsic directivities of the shear noise and self-noise. One may note that the isotropic directivity of self-noise is a necessary consequence of the isotropy of the turbulence.

The expression of the acoustical directional intensity for the total noise per unit volume of the jet appears as the sum of the shear and self-noise contributions:

$$I(x,\theta/\mathbf{y})=I^{\text{Se.N.}}(x,\theta/\mathbf{y})+I^{\text{Sh.N.}}(x,\theta/\mathbf{y}). \tag{15}$$

This total intensity can be put in the form:

$$[\underbrace{A}_{\text{Self-noise}}+\underbrace{B/2(\cos^4\theta+\cos^2\theta)}_{\text{Shear noise}}]\cdot\underbrace{1/C^5}_{\text{convection effect}}. \tag{16}$$

The self-noise contribution is radiated isotropically, while the shear noise has a dipolelike pattern. The combined pattern for $A=B=1$ is a quasiellipsoid with the long axis in the direction of the jet axis. As a consequence of the convection effect, the factor $1/C^5$ enhances the intensity in the downstream direction and largely attenuates the sound radiation in the upstream region. This effect is more exaggerated at high Mach numbers. To avoid oversimplification in this range, Ribner[6] and Ffowcs Williams[12] found it necessary to allow for variation of retarded time with source position. This led to a modified convection factor

$$C_m=[(1-M_c\cos\theta)^2+\alpha^2M_c^2]^{1/2}, \tag{17}$$

where $\alpha M_c=\omega_fL_1/(\sqrt{\pi}c_0)$. In Ribner[6] the coefficient α is taken equal to 0.55 while experiments of Davies *et al.*[15] indicate that α is closer to 0.3.

C. Goldstein model

The model devised by Goldstein[8] generalizes the Ribner model which has just been reviewed. It is argued by Goldstein that it is more appropriate to assume that the turbulence in the jet is axisymmetric. In fact the mean flow introduces a preferred direction so that the isotropic turbulence description is less adequate because it neglects important anisotropies such as the marked reduction in the transverse integral scale. As pointed out by Davies *et al.*[15] and Grant,[16] the large-scale eddies become mainly long cylindrical structures having a longitudinal scale approximately three times the transverse scale.

For brevity, we will only review in this section the assumptions which differ from those of Ribner's model and we will give the expressions of the acoustical directional intensity for the shear and self noise per unit volume of the jet.

(A1) The arbitrary time-independent tensor $R^0_{ijkl}(\mathbf{y}',\boldsymbol{\eta})$ is chosen as:

$$R^0_{ijkl}(\mathbf{y}',\boldsymbol{\eta})=U_1'^2\delta_{1i}\delta_{1j}\overline{u''_{tk}u''_{tl}}+U_1''^2\delta_{1k}\delta_{1l}\overline{u'_{ti}u'_{tj}}+U_1'^2U''^2\delta_{1i}\delta_{1j}\overline{u''_{1k}u''_{1l}}+\overline{u'_{ti}u'_{tj}u''_{tk}u''_{tl}}. \quad (18)$$

(A2) To treat the axisymmetric turbulence situation, it is necessary to introduce the point $\mathbf{y}$ defined by

$$\mathbf{y}=\left(y_1',\frac{y_2'+y_2''}{2},\frac{y_3'+y_3''}{2}\right). \quad (19)$$

According to this definition, $\mathbf{y}$ is not the midpoint of $\mathbf{y}'$ and $\mathbf{y}''$ as in the isotropic case.

(A3) For axisymmetric turbulence, the two-point correlation $R_{ij}(\mathbf{y},\boldsymbol{\xi},\tau)$ may be expressed in terms of two independent scalar functions:[17]

$$R_{ij}=\epsilon_{jlm}\frac{\partial q_{im}}{\partial \xi_l}, \quad (20)$$

where

$$q_{im}=\xi_k[\epsilon_{imk}Q_1+\epsilon_{i1k}(\delta_{1m}Q_2+\xi_mQ_3)], \quad (21)$$

$$Q_3=\left(\frac{\partial}{\partial\xi_1}-\frac{\xi_1}{\xi_3}\frac{\partial}{\partial\xi_3}\right)Q_1, \quad (22)$$

where ϵ_{jlm} is the antisymmetric symbol $1/2(j-l)(l-m)(m-i)$.

Kinematically acceptable models for Q_1 and Q_2 are

$$Q_1(\mathbf{y},\boldsymbol{\xi},\tau)=-\frac{1}{2}\overline{u_{t1}^2}f(\mathbf{y},\tau)\exp\left[-\left(\frac{\xi_{23}^2}{L_2^2}+\frac{\xi_1^2}{L_1^2}\right)^{1/2}\right], \quad (23)$$

$$Q_2(\mathbf{y},\boldsymbol{\xi},\tau)=-(\overline{u_{t2}^2}-\overline{u_{t1}^2})f(\mathbf{y},\tau)\exp\left[-\left(\frac{\xi_{23}^2}{L_2^2}+\frac{\xi_1^2}{L_1^2}\right)^{1/2}\right], \quad (24)$$

where

$$\xi_{23}^2=\xi_2^2+\xi_3^2. \quad (25)$$

Here, L_1 and $\overline{u_{t1}^2}$ (respectively, L_2 and $\overline{u_{t2}^2}$) are the longitudinal (respectively, transversal) integral scale and kinetic energy of the turbulence. The function f is not specified in Ref. 8. It is consistent to adopt a temporal Gaussian function for $f(\mathbf{y},\tau)$ as was done previously in the isotropic case:

$$f(\mathbf{y},\tau)=\exp(-\omega_f^2\tau^2). \quad (26)$$

The $\mathbf{y}$ dependence is implicit in ω_f.

By assuming that the axis of symmetry coincides with the axis of the jet and after some tedious calculations, the following expressions are obtained for the acoustical directional intensities per unit volume of the jet relative to the shear and self-noise:

$$I^{\mathrm{Se.N.}}(x,\theta/\mathbf{y})=\rho_0\frac{12L_1L_2^2}{5\pi c_0^5x^2}\overline{u_{t1}^2}^2\omega_f^4\frac{D_i^{\mathrm{Se.N.}}}{C^5}, \quad (27a)$$

where

$$D_i^{\mathrm{Se.N}}=\{1+2(M/9-N)\cos^2\theta\sin^2\theta+\tfrac{1}{3}[M^2/7+M-1.5N(3-3N+1.5/\Delta^2-\Delta^2/2)]\sin^4\theta\}, \quad (27b)$$

$$I^{\mathrm{Sh.N.}}(x,\theta/\mathbf{y})=\rho_0\frac{24L_1L_2^4\overline{u_{t1}^2}}{\pi c_0^5x^2}\left(\frac{\partial U_1}{\partial y_2}\right)^2\omega_f^4\frac{D_i^{\mathrm{Sh.N.}}}{C^5}, \quad (27c)$$

where

$$D_i^{\mathrm{Sh.N.}}=\cos^2\theta(\cos^2\theta+\tfrac{1}{2}[1/\Delta^2-2N]\sin^2\theta). \quad (27d)$$

In these expressions, the effect of the anisotropic structure of the turbulence appears through the following three parameters:

$$\Delta=L_2/L_1,\quad N=1-\overline{u_{t2}^2}/\overline{u_{t1}^2},$$

and (27e)

$$M=[1.5(\Delta-1/\Delta)]^2.$$

If one writes the expression of the total acoustical intensity in a form similar to relation (16), one finds that the self-noise contribution is now directional. The radiation pattern (for $\Delta=\frac{1}{3}$ and $N=\frac{1}{3}$) has a dipolar shape where the dipole axis is in the transverse direction ($\theta=90°$). The present shear noise radiation pattern resembles that of the Ribner model. Notice that in the limiting case of isotropic turbulence ($\Delta=1$ and $M=N=0$) the directivity expressions of (27b) and (d) become identical to those of Ribner.

D. Determination of the statistical properties of turbulence with a κ-ϵ model

To obtain estimates of noise radiation, it is necessary to specify the many statistical variables that appear in the previous models. In order to use the theoretical expressions (13), (14) and (27a) to (27d) of the directional acoustical intensity per unit volume $I(x,\theta/\mathbf{y})$, one has to provide the following local quantities:

- U_1 axial mean flow velocity,
- $\overline{u_{tm}^2}$, $\overline{u_{t1}^2}$, and $\overline{u_{t2}^2}$ mean, longitudinal, and transversal turbulent kinetic energy,
- L_1 and L_2 longitudinal and transversal integral scale of turbulence,
- ω_f angular frequency of turbulence,
- U_{1c} axial eddy convection velocity.

The quantities U_1 and $\overline{u_{tm}^2}$ are directly determined from a numerical solution of Reynolds average Navier–Stokes equations associated with a κ-ϵ turbulence model. Let us recall at this point that κ (dimensions of energy per unit mass) designates the turbulent kinetic energy of the flow while ϵ is the turbulent dissipation:

$$\epsilon=\mu \overline{\frac{\partial u_{ti}}{\partial x_j} \frac{\partial u_{ti}}{\partial x_j}}.$$

The dissipation ϵ has dimensions of energy per unit mass and per unit time. It is also worth remembering that the ratio κ/ϵ provides a typical time of the local turbulence while $\kappa^{\frac{3}{2}}/\epsilon$ yields a typical length scale. To evaluate the mean and turbulent aerodynamic variables, we use the axisymmetric version of the numerical code ULYSSE[18] developed by the "Département Laboratoire National d'Hydraulique" of the "Direction des Etudes et Recherches d'Electricité De France." Numerical results obtained for the mean flow velocity U_1 and for the turbulent energy $\overline{u_{tm}^2}$ were checked by comparing the numerical estimates with the data of Pao[7] and Davies *et al.*[15] These tests show that one can predict the self-similar behavior of the profiles of U_1 and $\sqrt{\overline{u_{tm}^2}}$, expressed in normalized variables in the mixing and developed region of the jet. Figure 2(a) and (b), respectively, display the spatial distributions of U_1 and κ for a nominal exhaust velocity U_{1j} equal to 195 m/s and for a nozzle diameter D of 0.025 m. It is known that the potential core length l_p (characterized by a constant axial velocity) extends over 4 to $5.5D$ depending on the exit characteristics of the turbulence. The mixing region is located between 0 to $4-5D$, followed by a transition zone which terminates at about $8-9D$. Beyond that point, the turbulent jet may be considered as fully developed. A careful analysis indicates that the numerical value of l_p is about $7D$ and thereby the mixing region is somewhat longer (extending to $7D$) than in the experiments. This shifts the transition region down to $11D$. This inaccuracy is encountered in Ref. 19 whereas it is shown in Ref. 20 that the standard κ-ϵ model do not substantially overpredict the length of the initial region. This error in the potential core length will have an effect on the jet noise prediction. The noise sources are shifted downstream and their typical scale and intensity is altered. However these inaccuracies are compensated by the semiempirical procedure explained in Sec. II A. Using an adjustable coefficient to match acoustic data for one set of conditions, one essentially absorbs the error made in estimating the potential length core. In Fig. 2(b) one recognizes the two mixing regions corresponding to the maximum of the turbulent energy κ. In fact the production of this quantity is intimately associated with velocity gradients which reach a maximum in the mixing regions and are negligible in the potential core. Due to the mechanism of turbulent diffusion, the thickness of the two mixing regions will grow and these two regions finally merge at about $10D$.

For the other aerodynamic and statistical quantities, we utilize the following closure relations:

(1) Based on the concept of turbulent viscosity, the expressions of $\overline{u_{t1}^2}$ and $\overline{u_{t2}^2}$ are

$$\overline{u_{t1}^2}=-2\nu_t \frac{\partial U_1}{\partial y_1}+\frac{2}{3}\kappa, \tag{28a}$$

$$\overline{u_{t2}^2}=-2\nu_t \frac{\partial U_2}{\partial y_2}+\frac{2}{3}\kappa, \tag{28b}$$

where $\nu_t=0.09\kappa^2/\epsilon$ is the kinematic turbulent viscosity.

(2) The integral scales should be in principle determined from spectral considerations. However simulations indicate that suitable estimates of L_1 and L_2 the longitudinal and transversal integral scales of turbulence may be specified in terms of κ and ϵ by:

$$L_1=\overline{u_{t1}^2}^{3/2}/\epsilon \quad \text{and} \quad L_2=\overline{u_{t2}^2}^{3/2}/\epsilon. \tag{29}$$

Now the numerical calculation leads to $\overline{u_{t1}^2} \approx \overline{u_{t2}^2} \approx \frac{2}{3}\kappa$ and as a consequence the scale L_2 becomes identical to L_1. This is so because the concept of turbulent viscosity is unable to correctly represent the splitting of the kinetic energy between the longitudinal and transversal directions.[21,22] In other words, the κ-ϵ turbulence model cannot predict the anisotropic distribution of length scales in the Goldstein model. It is already mentioned that in experiments the ratio $\Delta=L_2/L_1$ is equal to 1/3.[15,16] This value is imposed in our calculations. In doing so, one accounts for the turbulence anisotropy (admittedly in a crude way) and one may then fully exploit the Goldstein model.

(3) To model the angular frequency ω_f, it is natural to use[23]

$$\omega_f=2\pi\epsilon/\kappa. \tag{30}$$

The modeling adopted for L_1, L_2, and ω_f and relying on Eqs. (29) and (30) depends implicitly on proportionality factors. However the available experimental data do not enable a precise determination of these factors. It is then necessary to introduce a global adjustment factor in the expressions of the total acoustical intensity (F_A^R for Ribner and F_A^G for Goldstein). The specification of these global factors is discussed in Sec. II A.

(4) The κ-ϵ model cannot provide the eddy convection velocity U_{1c}. In general, this velocity is considered constant throughout the jet and is equal to 0.6–0.7 of the value of the mean jet exit velocity. In order to take into account the variation of this velocity is observed by Davies *et al.*,[15] we utilize his experimental profile obtained in the mixing region and expressed in reduced variables:

$$\frac{U_{1c}}{U_{\text{ref}}}=f\left[\left(y_1-\frac{D}{2}\right) \Big/ y_2\right],$$

where y_1 and y_2 are the axial and radial coordinates and the reference velocity is identified to the axial velocity $U_1(y_2=0)$. To estimate the local value of U_{1c} over the whole jet, we also assume that this profile is valid in the transition and developed region. We will show in the next section the advantage of this modeling when compared to the crude assumption U_{1c}=constant.

II. RESULTS AND COMPARISON FOR A SINGLE FREE JET

It is still necessary to explain how we determine the global adjustment factors and how we find the optimal set of expressions for the convection velocity and the coefficient α. We will then compare numerical results with the data reported by Lush.[10] We will consider first the evolution of the total acoustical power W emitted by the jet as a function of the jet exit velocity U_{1j} and we will then examine the distribution of acoustical intensity $I(x,\theta)$ in terms of the observation angle θ. Expressions relating W and $I(x,\theta)$ to $I(x,\theta/\mathbf{y})$ are as follows:

$$I(x,\theta)=\int_V I(x,\theta/\mathbf{y})d\mathbf{y}, \tag{31}$$

where $I(x,\theta/\mathbf{y})$ is obtained from Eq. (15)

$$W=2\pi x^2\int_{\theta_{\min}}^{\theta_{\max}} I(x,\theta)\sin\theta\, d\theta, \tag{32}$$

where $\{\theta_{\min}=7.5°,\ \theta_{\max}=105°\}$ is the range of variation of θ in the experiments.

Theoretically, the acoustical power must be integrated between 0° and 180°. However as noticed by Lush,[10] $I(x,\theta/\mathbf{y})$ is largely attenuated by the convection factor at large angles et by the factor $\sin\theta$ for the small angles (close to the jet axis). Thus the limitation of $\{\theta_{\min},\theta_{\max}\}$ to $\{7.5°,105°\}$ introduces a negligible error. As a matter of interest, in the experiments, the power attributed to the deleted $\theta_{\min}=7.5°$ cone will be almost entirely refracted out of this cone and thus be measured. It will, however, be small.

A. Determination of F_A^R, F_A^G, U_{1c}, and α

Let us recall (see Sec. I A), that one has to add the correction αM_c to the convection factor C for high jet velocities [Eq. (20)]. However different choices for α and U_{1c} are possible and one has to find the optimal choice. One also has to specify the global adjustment factor F_A^R and F_A^G for the two models. The procedure adopted is as follows:

For each model and for a specified choice of α and U_{1c}, the global adjustment factor is determinated so that the directional intensity at 90° $I(x,\theta=90°)$ coincides with the experimental value of Lush for one single velocity $U_{1j}=125$ m/s taken as reference. We then calculate the deviation D_W between the measured and numerical value of the total acoustic power W for $U_{1j}=300$ m/s and the optimal choice of rules is that which gives the minimum of D_W. Table I presents five possible choices, with the corresponding values of F_A and D_W for the two models. The optimal choice corresponds to the fifth group of rules R_5 where the deviation D_W observed is minimal. A close inspection of this table shows that much is gained by allowing for variations of the convection velocity. Because U_{1c} is a function of $\mathbf{y}$, the factor $1/C_m^5$ calculated therefore is also a function of source position and the final outcome is a derived jet-average $\langle 1/C_m^5\rangle$. At high subsonic jet speeds, it is indicated by a reviewer that this should yield a big improvement over the constant semiempirical $\langle 1/C_m^5\rangle$ factor.

TABLE I. Values of the adjustment factor F_c for the 2 models relative to five different groups of rules.

		Ribner model		Goldstein model	
		F_A^R (dB)[a]	D_W^R (dB)[b]	F_A^G (dB)[a]	D_W^G (dB)[b]
R_1	$U_{1c}=0.67U_{1b}$ $\alpha=0$	-16.2	7.3	-27.9	4.2
R_2	$U_{1c}=0.67U_{1b}$ $\alpha=0.3$	-16.1	6.0	-27.8	3.1
R_3	$U_{1c}=0.67U_{1b}$ $\alpha=0.55$	-16.0	3.5	-27.6	1.0
R_4	$U_{1c}=0.67U_{1b}$ $\alpha=\omega_f L_1/\sqrt{\pi}U_{1c}$	-16.1	5.1	-27.7	2.3
R_5	$U_{1c}=$ Davies *et al.* profile $\alpha=\omega_f L_1/\sqrt{\pi}U_{1c}$	-16.1	2.5	27.7	0.2

[a] $F_A=I(x,\theta=90)_{\text{Lush}}-I(x,\theta=90)_{\text{code}}$ at 125 m/s.
[b] $D_W=W_{\text{Lush}}-W_{\text{code}}$ at 300 m/s.

Thus all the calculations presented in the next sections for these adapted models of Ribner and Goldstein correspond to the fifth group of rules R_5. These adapted two models will be, respectively, designated by R_a and G_a.

B. Total acoustical power

Numerical calculations correspond to four jet exit velocities: 90, 125, 195, and 300 m/s. Figure 3 shows that the

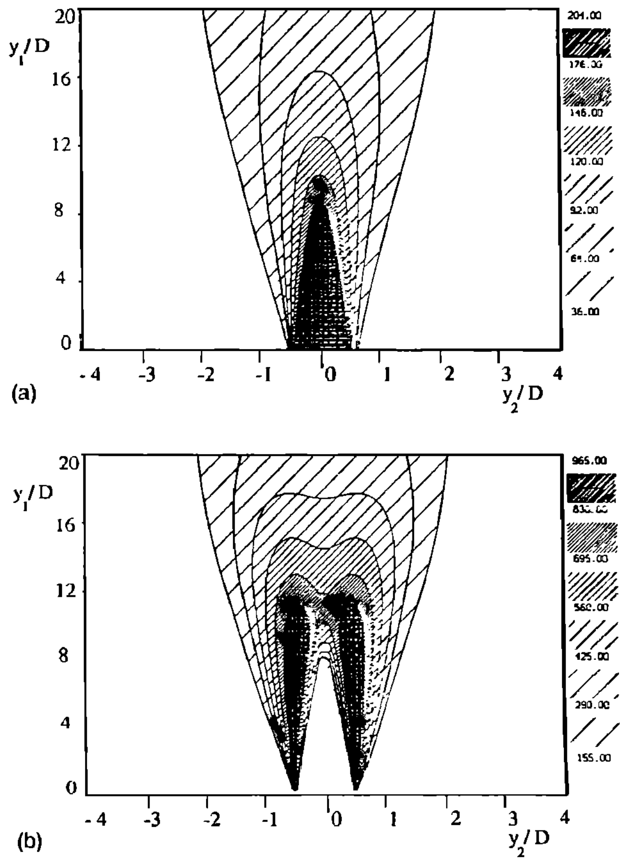

FIG. 2. Spatial distribution of the axial mean velocity U_1 and the turbulent kinetic energy κ for $U_{1j}=195$ m/s. (a) Axial velocity U_1 (m/s). (b) Turbulent kinetic energy κ (m^2/s^2). The scale of gray levels shown on the right side of the figures is used to plot the distributions. For example, the darkest symbol on (a) corresponds to values between 176 and 204 m/s. Nozzle lips are located at $y_1/D=0$ and $y_2/D=\pm 1/2$.

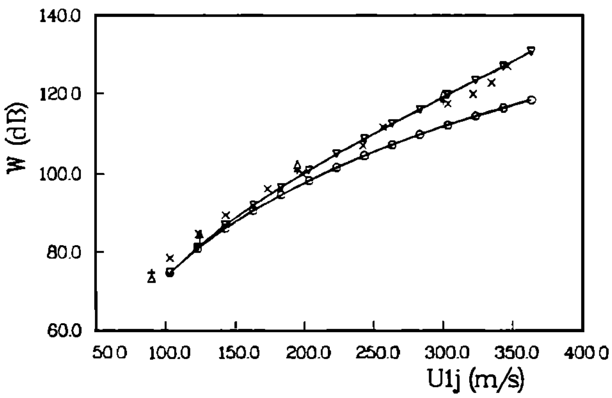

FIG. 3. Variation of the total acoustic power W as a function of jet exit velocity U_{1j} [○: U_{1b}^8 law, △: R_a model, +: G_a model, ×: Lush data, ▽: relation (33)]. The acoustic power is expressed in dB, *re*: 10^{-12} W.

model G_a correctly predicts the evolution of the total acoustic power and closely follows the data of Lush. The deviation D_W at 300 m/s is about 0.2 dB, while this deviation is 2.5 dB for the R_a model.

The same figure also displays the standard U_{1j}^8 law. This scaling law initially proposed by Lighthill indicates that the acoustic efficiency defined as the ratio of the acoustic power to the mechanical power of the jet increases like M^5. The U_{1j}^8 law does not apply in the supersonic range. It is known for example that the sound power radiated from jets exhausting from rockets increases like the third power of the velocity. In the high speed range the acoustic efficiency is roughly constant (this efficiency is typically equal to 0.5%). One finds that the U_{1j}^8 law closely follows the variation of the acoustic power for velocities less than 250 m/s. In the high subsonic range it appears that the acoustic efficiency is a function of the Mach number. In this range the effect of convection becomes important and according to[10] the dimensional relation U_{1j}^8 is replaced by

$$W \sim \rho_0 U_{1j}^8 \frac{D^2}{c_0^5} \frac{1+M_c^2}{(1-M_c^2)^4}. \tag{33}$$

This law is singular at $M_c=1$ because it results from integrating the singular factor $1/C^5$ of Lighthill over a unit sphere. By contrast, the corresponding integral of the nonsingular factor I/C_m^5 of Ribner and Ffowcs-Williams is itself nonsingular. Expression (33) is also plotted in Fig. 3 ($M_c=0.67\ U_{1j}/c_0$, is used in the calculation). The experimental values are correctly predicted by this expression when the jet velocity exceeds 250 m/s (see Fig. 3). All the results are expressed in decibel units with a reference power of 10^{-12} W. Intensity levels given below are also expressed in decibels with a reference intensity of 10^{-12} W/m^2.

C. Acoustical directional intensity

Relations (31), (15) together with (13)–(14) or (27) provide the acoustical intensity $I(x,\theta)$ due to the jet in the observation direction θ. Figure 4(a), (b), and (c) display this intensity for the two models compared to the data of Lush and for three jet exit velocities 125, 195, and 300 m/s. The overestimation of the intensity $I(x,\theta)$ by the R_a model increases as the velocity increases and may reach up to 5 dB at the very small angles ($\theta \sim 20°$). However at these angles, the G_a model yields suitable predictions of $I(x,\theta)$ for the two velocities 195 and 300 m/s and underestimates the intensity level for 125 m/s. Later on we will explain the reason for the deficiency of the G_a model at this velocity. This model is the most accurate in the high subsonic range (typical exhaust velocities of about 300 m/s) when compared to others models based on the Lighthill's theory. While this conclusion holds, it is also true that the R_a model would have come closer to experimental points if we had matched at 45° and at the intermediate velocity of 195 m/s. Figure 4(d) includes, in addition to the R_a and G_a results, the predictions of $I(x,\theta)$ obtained from the following models.

(1) A first set of estimates is obtained from a simplified model based on dimensional considerations and providing an algebraic expression for the directional intensity:

$$I(x,\theta) \sim \rho_0 \frac{U_{1j}^8}{c_0^5} \frac{D^2}{x^2} \frac{1}{(1-M_c \cos\theta)^5}, \tag{34}$$

where $M_c=0.67\ U_{1j}/c_0$. This model is used by Lush[10] in comparisons with experimental data.

(2) A second set of predictions is generated with a model due to Bilanin *et al.*[9] based on the second version of Ribner's theory[5] including an improved formulation of $U_1'U_1''$ similar to the one adopted in our own R_a model. The mean flow and the statistical turbulent properties are obtained from a κ-l turbulence closure, where l is a characteristic length of turbulence. The expressions for the acoustical directional intensity for the self- and shear noise are

$$I^{\text{Se.N.}}(x,\theta/y) = K_1 \frac{\rho_0}{4\pi c_0^5 x^2} \frac{l^3 \overline{u_{lm}^2}^2 \omega_f^4}{C_m^5}, \tag{35a}$$

$$I^{\text{Sh.N.}}(x,\theta/y) = K_2 \frac{\rho_0}{4\pi c_0^5 x^2} \frac{l^4 \overline{u_{lm}^2} \omega_f^4}{C_m^5} U_1 \frac{\partial U_1}{\partial y_2} \times (\cos^4\theta + \cos^2\theta), \tag{35b}$$

where K_1, K_2 are numerical constants. Notice that expression (35a) is identical to the expression of the self-noise in Ribner's model (13). However, expressions for the shear noise (35b) and (14) exhibit two important differences:

(i) In the convection factor C_m, the axial convection velocity U_{1c} is approximated by the mean axial velocity U_1.

(ii) The intensity of shear noise is now proportional to $l^4 U_1(\partial U_1/\partial y_2)$ in (35b) instead of $l^5(\partial U_1/\partial y_2)^2$ as in (14). We will show in this section that these differences restrict the predictive capability of this model.

(iii) A third group of values is determined with a model due to Hecht *et al.*[24] In this model, the two-point correlation $R_{ij}(\xi,\tau)$ is directly calculated from the solution of an equation governing this correlation in the case of an homogeneous turbulence with a mean flow submitted to unidirectional constant shear.

Figure 4(d) shows that Bilanin's model is no better than the simplified expression (34). Our R_a model based on a more refined noise generation description is more accurate.

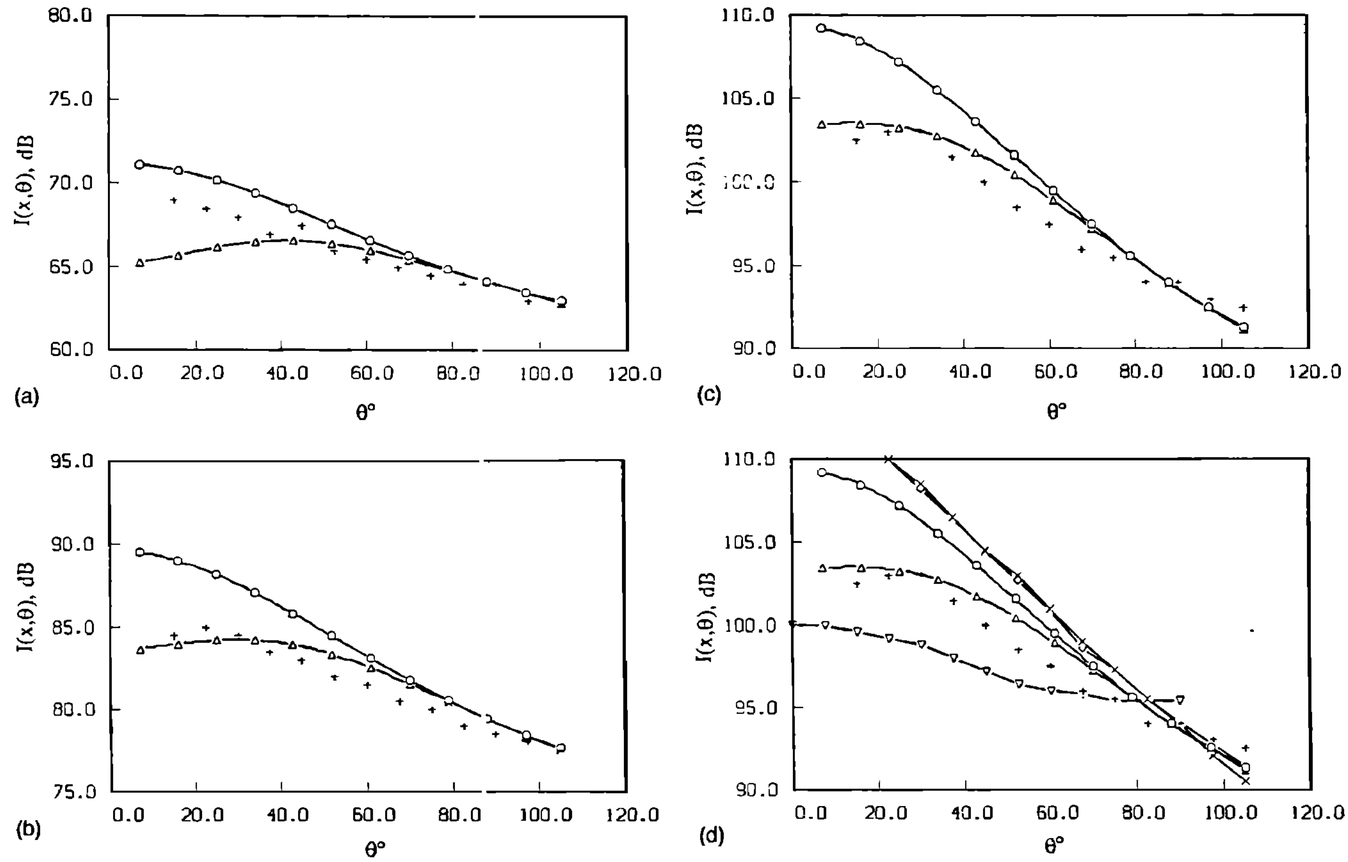

FIG. 4. Variation of the acoustic directional intensity of total noise as a function of the angle of observation θ for the two models R_a and G_a. (a) $U_{1j}=125$ m/s, (b) $U_{1j}=195$ m/s, (c) $U_{1j}=300$ m/s, (d) $U_{1j}=300$ m/s. (O: R_a model, Δ: G_a model, +: Lush data, $\times$: simplified model, $\Diamond$: estimates generated with the model due to Bilanin, ∇: estimates generated with the model due to Hecht. The meaning of the symbols in this figure differs from that used in Fig. 2. Note that the last three symbols are only used in (d).

On the other hand, although the Hecht approach looks promising, the hypothesis of uniform shear and the use of a large set of closure assumptions of the governing equation of $R_{ij}(\xi,\tau)$ finally limits the performance of this scheme. One finds in particular [Fig. 4(d)] that the Hecht model underestimates the intensity at small angles θ.

In order to refine our analysis of the variation of $I(x,\theta)$ as a function of θ, we have calculated the two contributions of self- and shear noise. The directional acoustical intensities for these two contributions due to the whole jet are

$$I^{\text{Se.N.}}(x,\theta)=\int_V I^{\text{Se.N.}}(x,\theta/\mathrm{y})d\mathrm{y}, \tag{36a}$$

$$I^{\text{Sh.N.}}(x,\theta)=\int_V I^{\text{Sh.N.}}(x,\theta/\mathrm{y})d\mathrm{y}, \tag{36b}$$

where $I^{\text{Se.N.}}$ and $I^{\text{Sh.N.}}(x,\theta/y)$ are given by Eqs. (13), (14) and (27a), (27c), respectively, for the two models R_a and G_a. As the expressions of the shear noise [see Eqs. (14) and 27(c)] feature a cos θ dependence, one finds (Figs. 5 and 6) that the self-noise intensity coincides with the total noise intensity at $\theta=90°$. In the case of the R_a model, the self-noise intensity having basically a uniform directivity, shows an amplification at small angles due to the convection factor $1/C^5$. If one adds the shear noise contribution which is not negligible for $\theta<45°$, the amplification becomes more pronounced in the total intensity and this explains why the R_a model overestimates the acoustical intensity in the range of small angles (Fig. 5).

In contrast, the two contributions of self and shear noise are complementary in the G_a model. For angles $\theta>45°$ (respectively, $\theta<45°$), the self-noise (respectively, shear noise) dominates so that the total intensity comes close to the measurements (see Fig. 6) except for the lowest velocity 125 m/s at small angles. In fact we must recall that one has imposed a fixed value $\frac{1}{3}$ to the ratio Δ of turbulent scales. While this is appropriate in the high velocity range, one expects that this ratio will tend to one for lower velocities because turbulent structures become more isotropic. If the variations of Δ were taken into account, the shear and self-noise directivities would approach those of the R_a model and the predictions would be improved at these small angles. From here on, we only discuss the results of the G_a model.

D. Spatial and frequency distribution of acoustical sources

In order to have a description of the spatial distribution of the acoustical sources in the jet, one has to invert the integration order. Starting from expressions (27) for the directional intensity $I(x,\theta/\mathrm{y})$ and integrating over θ, one obtains the acoustic power generated by the unit volume of the jet:

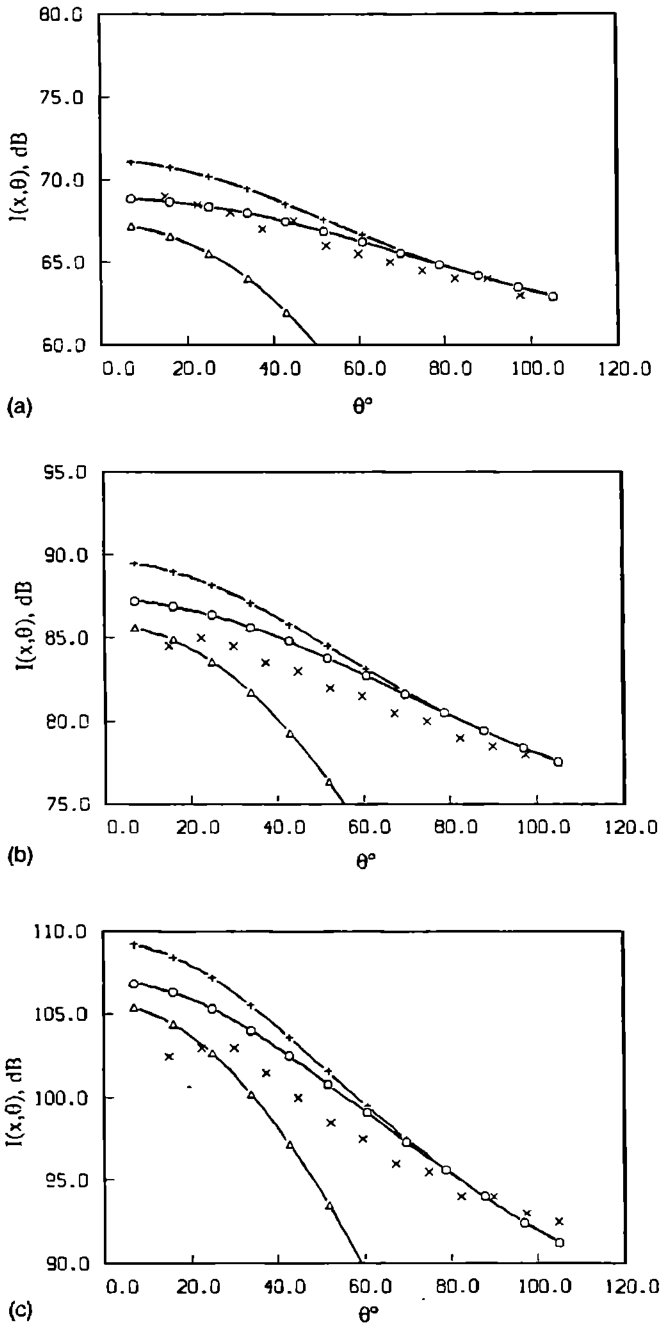

FIG. 5. Variation of the acoustic directional intensity of self-noise and shear noise as a function of the angle of observation θ for the R_a model. (a) $U_{1j}=125$ m/s; (b) $U_{1j}=195$ m/s, (c) $U_{1j}=300$ m/s (O: self-noise, Δ: shear noise, +: total noise, ×: lush data).

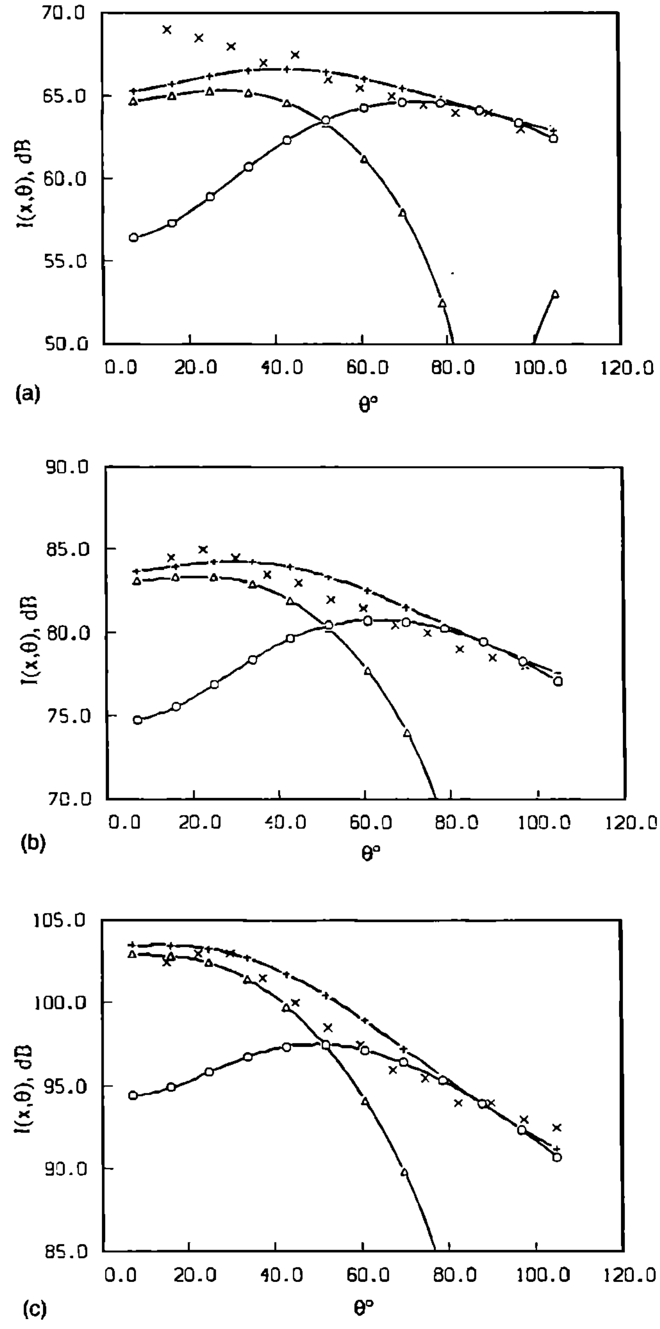

FIG. 6. Variation of the acoustic directional intensity of self-noise and shear noise as a function of the angle of observation θ for the G_a model. (a) 125 m/s, (b) 195 m/s, (c) 300 m/s (O: self-noise, Δ: shear noise, +: total noise, ×: lush data).

$$W(/\mathbf{y})=2\pi x^2\int_{\theta\ \min}^{\theta\ \max} I(x,\theta/\mathbf{y})\sin\,\theta\, d\theta. \tag{37}$$

It is obvious that the integral of $W(/\mathbf{y})$ over the jet gives the total power W as given by expression (32). As a check we have tested this equivalence. Fig. 7, corresponding to an exit velocity of 195 m/s, provides a typical spatial distribution of the acoustic power in a range extending from $W_{\max}(/\mathbf{y})-15$ dB to $W_{\max}(/\mathbf{y})$. This figure indicates that the acoustic sources are localized between 0 and $12D$, e.g., in the mixing and transition regions. In fact, the amplitude of self- and shear noise are proportional to the intensity of turbulence and shear gradients which are important in these regions. This clearly shows that the noise contributions of the potential core and developed regions are not significant.

To obtain the exact percentage of acoustic power generated in each region of the jet, we have calculated a longitudinal distribution function $F_w(y_1)$ of the acoustic power defined as

$$F_W(y_1)=\frac{1}{W}\int_0^{y_1} dy_1\int_V W(/\mathbf{y})dy_2\, dy_3. \tag{38}$$

This function was determined for $U_{1j}=125$, 195, and 300 m/s. Table II displays the values of $F_W(y_1)$ for $y_1/D=7$

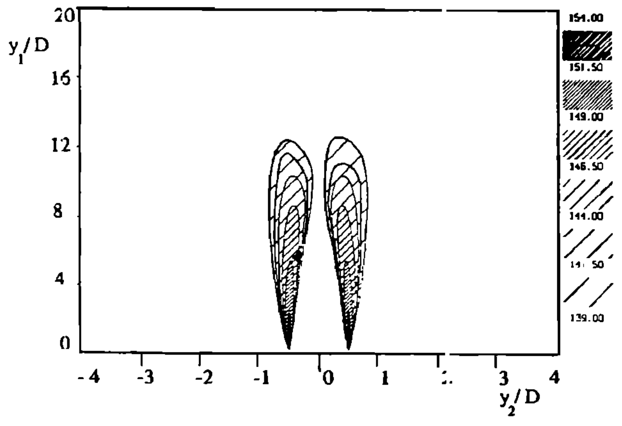

FIG. 7. Spatial distribution of the acoustic power $W(\mathbf{y})$ per unit volume of the G_a model for $U_{1j}=195$ m/s. The acoustic power s expressed in dB, *re*: 10^{-12} W.

and 11. From these values, one may conclude that 60% of the acoustic power is emitted from the mixing region ($y_1<7D$) and 30% originates from the transition region. This confirms the Ribner,[5] Crighton,[25] and Goldstein[26] assertions that the two regions contribute the main part of the jet noise emission.

Now, we examine the expression of the acoustical power spectrum $W_\omega(/\mathbf{y})$ per unit volume of the jet to describe the frequency distribution of the acoustical sources:

$$W_\omega(/\mathbf{y})=2\pi x^2\int_{\theta\,\min}^{\theta\,\max} I_\omega(x,\theta/\mathbf{y})\sin\theta\, d\theta, \tag{39}$$

where $I_\omega(x,\theta/\mathbf{y})$ is the directional acoustical intensity spectrum obtained by taking a Fourier transform of the autocorrelation function $C_{\rho\rho}(x,\theta/\mathbf{y},\tau)$ (see the Appendix). The spatial distribution of $W_\omega(/\mathbf{y})$ is represented in Fig. 8(a) to (d) for $U_{1j}=125$ m/s and for four frequencies corresponding to Strouhal numbers $\mathrm{St}=\omega D/(2\pi U_{1j})=0.03$, 0.3, 1.0, and 3.0. At the low frequency (St=0.03), the sources are in the developed region, while at the high frequency (St=3.0) they are in the mixing region near the nozzle. In the intermediate frequency range (St=0.3 and 1.0) the sources are located between the end of the mixing region and the beginning the developed region. In fact, the small eddies formed near the nozzle and convected at high speed in the initial shear layer are responsible for the high-frequency emission while the larger eddies which develop further downstream have a decreasing typical frequency and therefore a lower emission frequency. Finally, if one defines a frequency distribution function $F_W(\mathrm{St})$ in terms of the Strouhal number, Table III indicates that about 40% of the power emitted is observed for St≤1.0 while 10% of the power is detected for St≥3.0.

TABLE II. Values of the spatial distribution function $F_W(y_1)$.

y_1/D	125 m/s	$F_W(\%)$ 195 m/s	300 m/s
7	57	60	59
11	89	89	93

III. PARAMETRIC STUDY OF TWO COAXIAL JETS

In order to test the predictive qualities of the present approach, we now apply the G_a model to the case of noise emission from coaxial jets. It is known that in such aerodynamic configurations, the noise emission depends on the secondary jet velocity. The exact behavior is nicely characterized in well-controlled experiments reported by Juvé *et al.*[11] Other experimental data are also available (for example, Ref. 27) but the aerodynamic field is not provided in that last reference while it is well documented by Juvé *et al.* The experiment carried on two coaxial jets at subsonic velocities and ambient temperature shows that the acoustic emission first diminishes as the secondary jet velocity is increased, reaching a minimum and then increasing again as the jet velocity is augmented further. Our goal is to predict the minimum of the acoustic emission as provided by this experiment.

A. Configuration studied

Figure 9 gives a schematic representation of Juvé's configuration. The exit velocity U_{1p} of the primary jet is held constant at 130 m/s, while the exit velocity U_{1s} of the secondary jet is varied from 0 to 91 m/s. Denoting by λ the ratio U_{1s}/U_{1p}, the selected values of this ratio are 0, 0.2, 0.4, 0.6, and 0.7. The diameters of the primary and secondary nozzles are, respectively, $D_p=30$ mm and $D_s=100$ mm.

The method adopted to calculate the acoustic emission for each value of λ is based first on a determination of mean and turbulent flow characteristics utilizing the numerical code ULYSSE. In a second step, using the G_a model, we determine the directional intensity $I(x,\theta)$ which is then compared to the experimental data of Juvé *et al.*[11] This intensity is measured at $\theta=90°$ at a distance $x=2.5$ m from the primary nozzle center. One may notice that for this particular angle the exact knowledge of the convection velocity profile U_{1c} is not crucial. The amplification C_m factor as shown by Eq. (20) becomes negligible for $\theta=90°$. This is confirmed by the constancy of the adjustment factor F_A in the case of a simple jet (see in Table I).

B. Numerical results

It has been verified[14] that the predicted aerodynamic results closely follow the data of Juvé *et al.*[11] Good agreement is obtained between numerical and measured transverse profiles for the axial mean flow velocity U_1 and the longitudinal kinetic turbulent energy $\overline{u_{t1}^2}$. Figure 10(a) to (d) shows the spatial distribution of the kinetic turbulent energy κ for four ratios 0.2, 0.4, 0.6, and 0.7. For a velocity ratio λ=0.2 the spatial distribution is essentially identical to the case of simple jet structure as may be seen by comparing [Figs. 2(b) and 10(a)], but the maximum of κ is lower as expected. Increasing the exit velocity U_{1s} of the secondary jet, one observes a shift of the maximum toward regions where the velocity gradients are the largest such as the primary-secondary mixing region and the zone located downstream of the primary jet potential core [Fig. 10(b)–(d)]. Notice that in Fig. 10(a), one cannot see the shear layer in the initial region between primary and secondary flows. This is due to

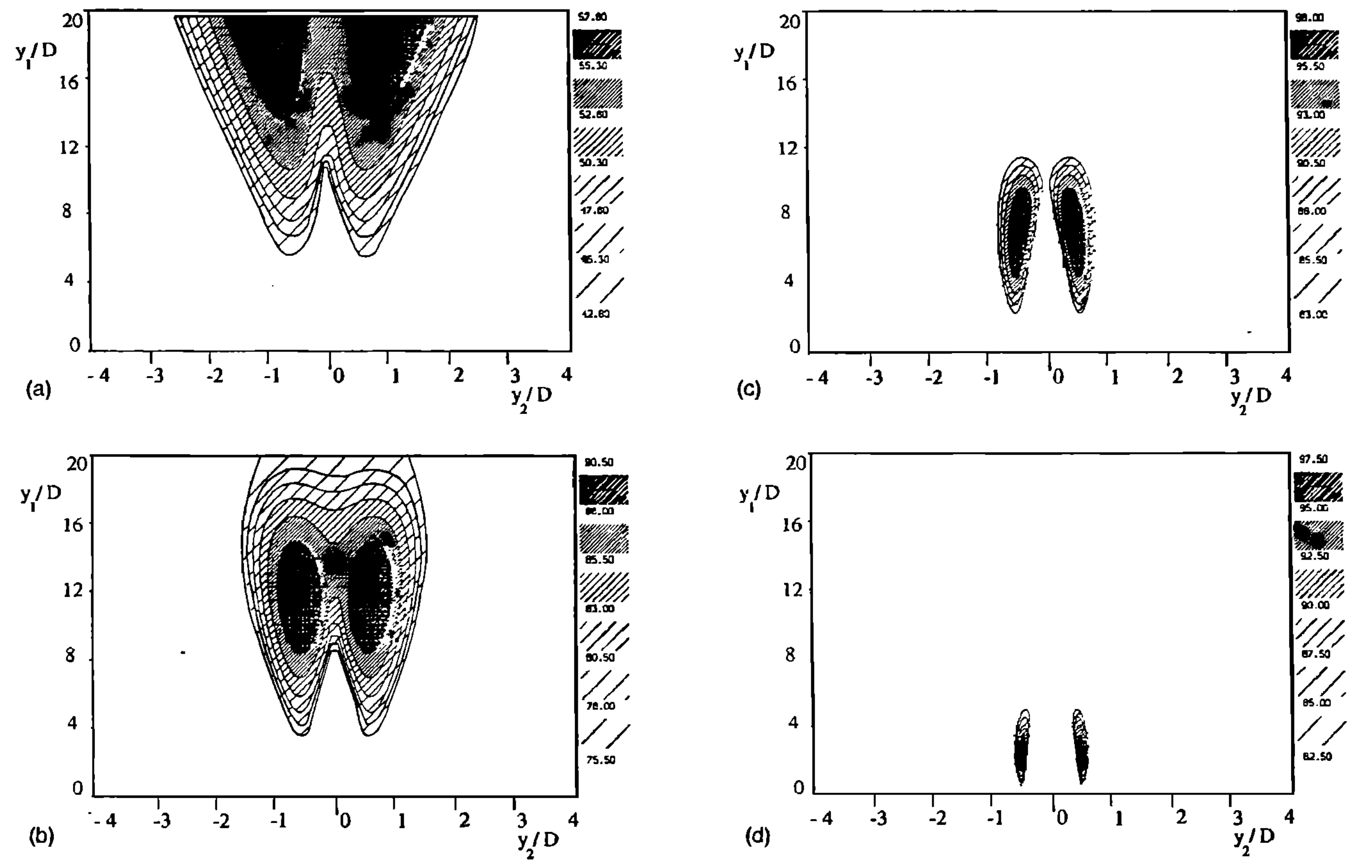

FIG. 8. Spatial distribution of the acoustic power spectrum $W_\omega(/y)$ per unit volume of the G_a model for $U_{1j}=195$ m/s. The acoustic power spectrum is expressed in dB, *re*: 10^{-12} W Hz^{-1}. (a) St=0.03, (b) St=0.3, (c) St=1.0, (d) St=3.0.

the fact that the level contours start from 50 to the maximum value 326. This means that the level of the turbulent intensity is below 50. This observation might be verified in Fig. 10(b). By increasing the secondary velocity ($\lambda=0.04$), the intensity of turbulence increases to a level between 40 and 70 [Fig. 10(b)].

The numerical calculations for $I(x,\theta)$ were carried out for five velocity ratios (see Fig. 11). In the case of the simple jet ($\lambda=0$) we observe a deviation of about 1.3 dB from the data. To interpret this finding it is worth comparing the experimental data of Lush and Juvé *et al.* This may be done by scaling one experiment (that of Lush[10]) to take into account the slight difference in diameter, jet velocity and distance of observation [*In Lush*: $D_L=25$ mm, $U_{1p}=125$ m/s, $x=3$ m, $\theta=90°$, and $I_L(x,\theta)$ is 64.0 dB while *in Juvé et al.* $D_J=30$ mm, $U_{1p}=130$ m/s, $x=2.5$ m, $\theta=90°$, and $I_J(x,\theta)$ is 69.4 dB]. To compare the two intensity values, we use the dimensional law $U^8\,D^2/x^2$ and obtain:

TABLE III. Values of the frequency distribution function $F_W(\mathrm{St})$.

St	$F_W(\%)$ 125 m/s	195 m/s	300 m/s
1	46	42	36
3	89	89	91

$$I_L^S=I_L+10\,\log_{10}\left(\frac{130}{125}\right)^8+10\,\log_{10}\left(\frac{30}{25}\right)^2$$
$$-10\,\log_{10}\left(\frac{2.5}{3.0}\right)^2=68.5\ \text{dB},$$

where I_L^S is the scaled Lush intensity and the deviation $(I_J-I_L^S)$ is 0.9 dB. One has to remember that the G_a model uses an adjustment factor F_A^G based on the experiment of Lush. Hence it is suitable to diminish the experimental values of Juvé *et al.* by 0.9 dB. This correction is incorporated in Fig. 11. In this figure, one sees that the G_a model retrieves the value $\lambda=0.4$ for which the acoustic intensity is minimum. The attenuation with respect to the single jet case, is 6.9 dB, while the measured value is 7.9 dB. The differences

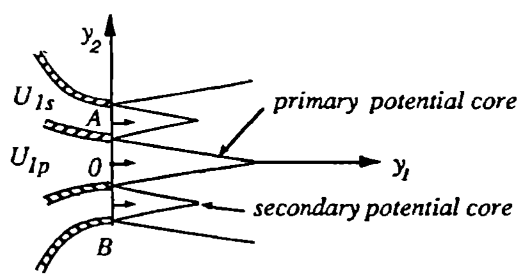

FIG. 9. Coaxial jet configuration. (U_{1p} and U_{1s} velocities of primary and secondary jets at the nozzle, D_p and D_s diameters of the inner and outer nozzles: $2\,OA=D_p$, $2\,OB=D_s$.)

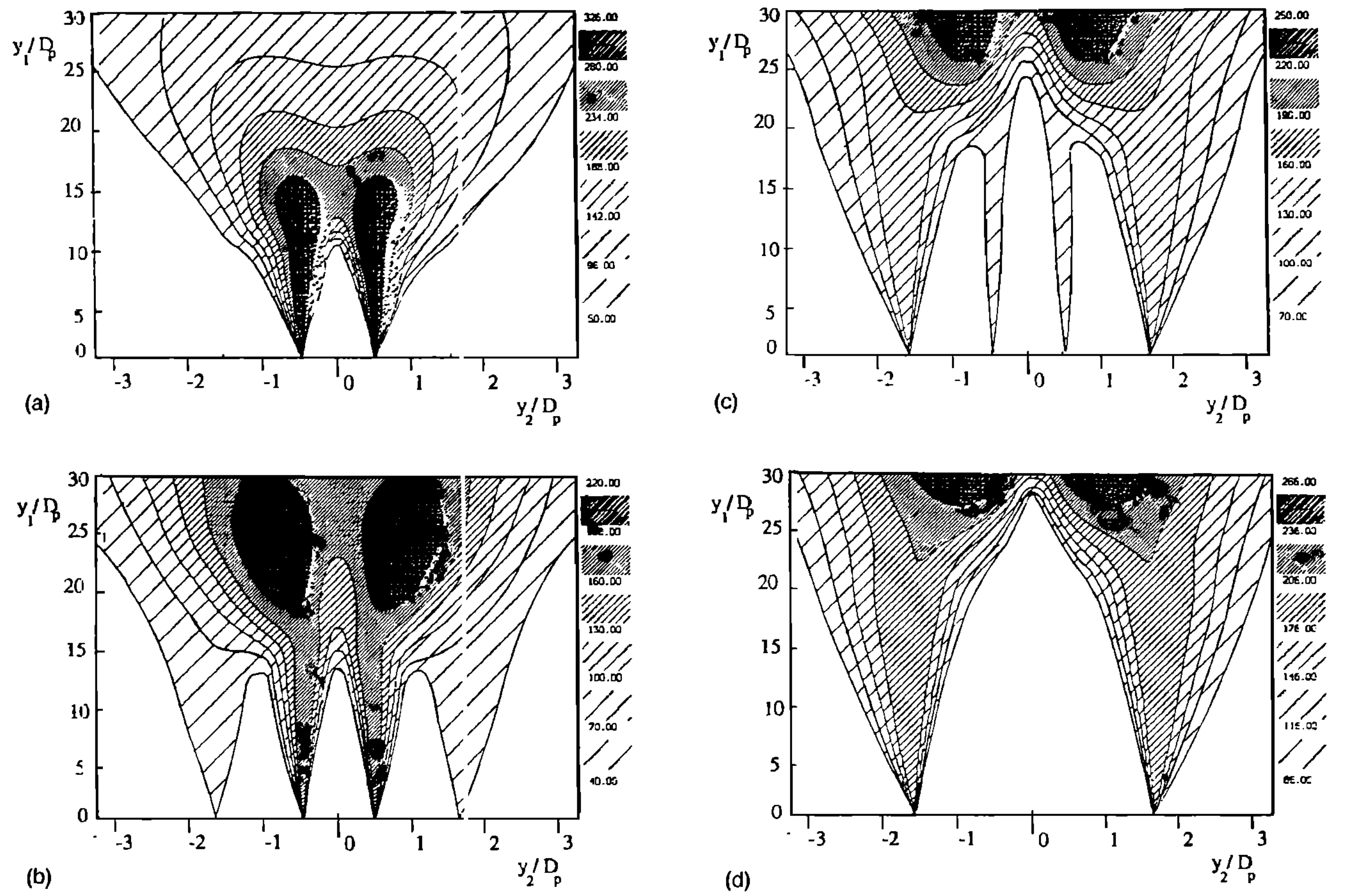

FIG. 10. Spatial distribution of the turbulent kinetic energy K for $U_{1p}=130$ m/s. (a) $\lambda=0.2$, (b) $\lambda=0.4$, (c) $\lambda=0.6$, (d) $\lambda=0.7$. Nozzles lips are located at $y_1/D_p=0$. The primary jet is between $-1/2<y_2/D_p<1/2$. The secondary jet nozzle lips correspond to $y_2/D_p=\pm 5/3$.

which are observed for $\lambda=0.6$ and 0.7 are due to the fact that some of the acoustical sources are progressively located outside of the computational domain. Indeed this domain extends over 30 D_p but this length is somewhat insufficient at the higher secondary jet velocities. This point is apparent in Fig. 12 which provides the spatial distributions of the acoustic power W (/y) per unit volume. This figure shows that for $\lambda=0.6$ and 0.7, a part of the acoustic power is still not represented. The figure also shows that the spatial distribution of

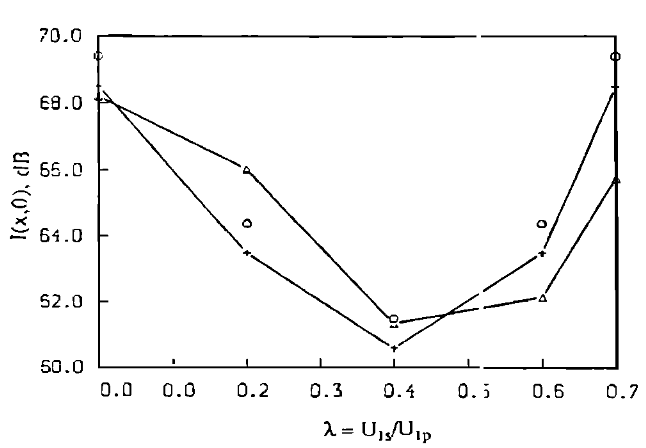

FIG. 11. Comparison between numerical acoustic directional intensity (G_a model) and experimental values of Juvé *et al.* for $\theta=90°$ and $x=2.5$ m (O: Juvé data, △: G_a model, +: Juvé corrected data).

sources remains similar to that of a simple jet up to $\lambda=0.4$ [Fig. 12(a) and (b)]. For $\lambda=0.6$ and $\lambda=0.7$ [Fig. 12(c) and (d)], one may observe the attenuation of acoustic sources in the primary-secondary jet mixing region and the presence of sources in the secondary jet mixing region and in the downstream region of the primary potential core.

IV. CONCLUSIONS

It is shown in this study that it is possible to estimate the noise emission of free turbulent jets from a numerical description of the mean and turbulent characteristics of the flow. Using a κ-ϵ turbulence model associated with jet noise models based on Lighthill's theory, two formulations have been used: Ribner's formalism postulates locally isotropic turbulence superposed on mean flow while Goldstein/Rosenbaum's formalism generalizes this to accommodate the more realistic assumption of axisymmetry. The results have correctly reproduced the evolution of the total acoustic power as a function of the jet exit velocity and the variation of the directional acoustical intensity as a function of the angle of observation. It is shown that the acoustic model (G_a model) deduced from the work of Goldstein is more accurate than the model relying on Ribner's analysis (R_a model). Furthermore, we show that the G_a model provides the best estimates of the directional acoustical intensity when compared to others models based on Lighthill's theory.

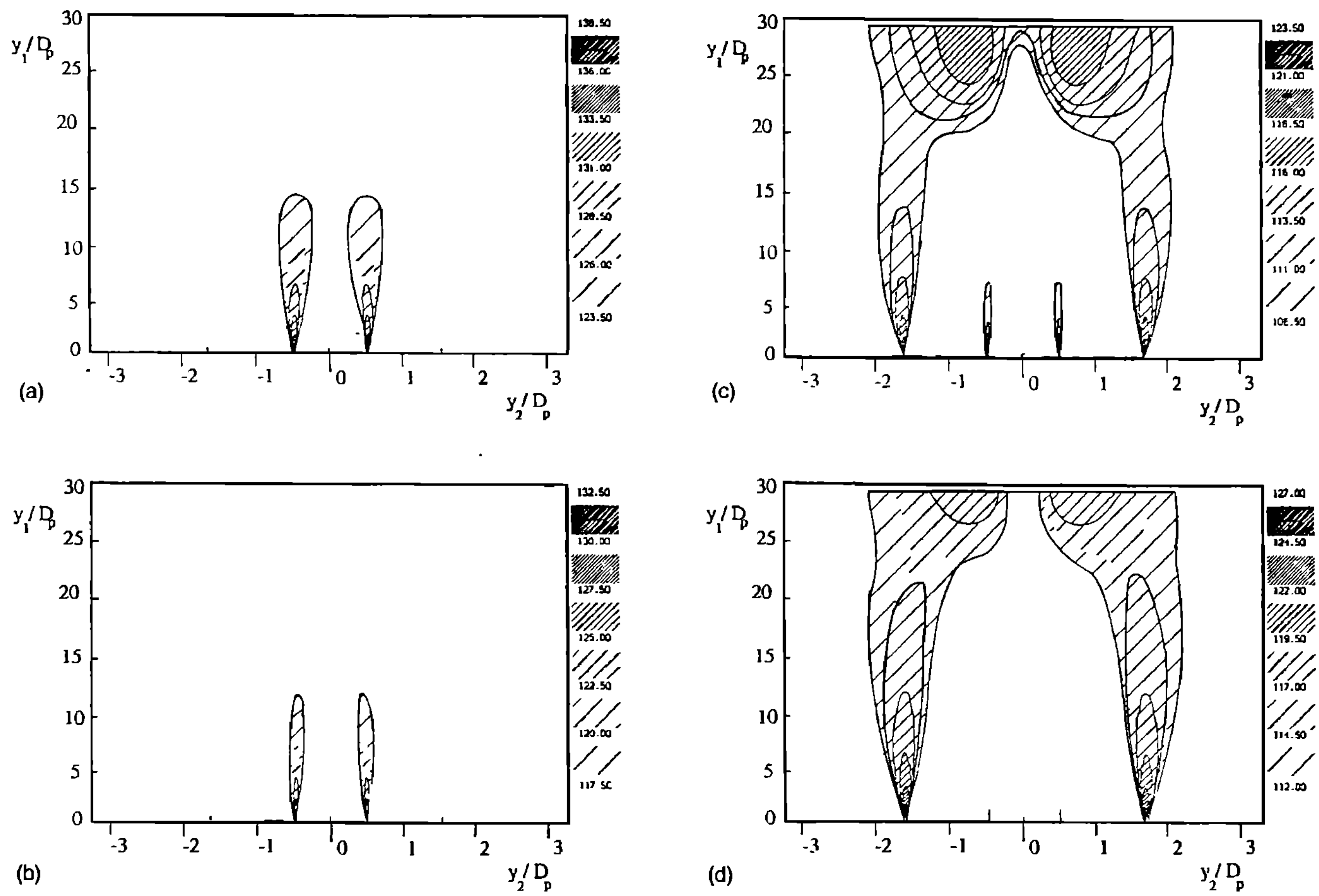

FIG. 12. Spatial distribution of the acoustic power spectrum $W_\omega(/\mathbf{y})$ per unit volume of the G_a model for $U_{1p}=130$ m/s. The acoustic power is expressed in dB, *re*: 10^{-12} W Hz^{-1}. (a) $\lambda=0.2$, (b) $\lambda=0.4$, (c) $\lambda=0.6$, (d) $\lambda=0.7$.

With this approach, we have obtained a complete picture of the spatial and frequency distribution of acoustical sources in the jet. We have shown in particular that the mixing and transition region are responsible for 90% of the acoustic power emitted and that these regions correspond, respectively, to the high and intermediate frequency radiation of sound.

This detailed description is useful in more complicated jet configurations. This point is illustrated in this study in the case of two coaxial jets. We have calculated the modifications of the characteristics of turbulence due to the variation of the secondary jet exit velocity, and have shown how these modifications govern the distribution of acoustic sources. One may notice in this case that the G_a model is applied without any changes. This indicates the generality of this approach and the possibility of its utilization in others jet geometries. However the quality of the noise estimates essentially depends on a better determination of the flow characteristics. An improvement could be obtained by using more advanced turbulence closures such as the Reynolds stress-dissipation R_{ij}-ϵ models, which in principle predict more precisely the distribution of the kinetic turbulent energy in the axial and transverse directions. With this kind of turbulence modeling, one may obtain better representations of the two parameters N and Δ of the G_a model.

Finally we have to recall that this model is unable to represent the phenomenon of refraction due to mean flow gradients. This phenomenon is mainly observed for high jet velocities at angles which are close to the jet axis ($\theta<25°$).

ACKNOWLEDGMENTS

We wish to thank the anonymous referees of this article and the associate editor (L. C. Sutherland) for their many helpful suggestions.

APPENDIX: DETERMINATION OF THE ACOUSTICAL INTENSITY SPECTRUM

The acoustical intensity spectrum $I_\omega(\mathbf{x})$ is obtained by applying the temporal Fourier transform of the density autocorrelation $C_{\rho\rho}(\mathbf{x},\tau)$ defined in the relation (4):

$$I_\omega(\mathbf{x})=\frac{1}{2\pi}\int_{-\infty}^{+\infty} C_{\rho\rho}(\mathbf{x},\tau)e^{j\omega\tau}\,d\tau, \tag{A1}$$

where $j^2=-1$ and ω designates the angular frequency. Let us denote W, $W_\omega(/\mathbf{y})$, $I_\omega(x,\theta/\mathbf{y})$, respectively, the total acoustical power, the acoustical power spectrum (emitted from a unit volume located at $\mathbf{y}$), and the directional acoustical intensity spectrum:

$$W=\int_V\int_{-\infty}^{+\infty} W_\omega(/\mathbf{y})d\mathbf{y}\,d\omega, \tag{A2}$$

$$W_\omega(/\mathbf{y})=2\pi x^2\int_0^\pi I_\omega(\mathbf{x},\theta/\mathbf{y})\sin\theta\, d\theta, \tag{A3}$$

$$I_\omega(\mathbf{x},\theta/\mathbf{y})=\frac{1}{2\pi}\int_{-\infty}^{-\infty} C_{pp}(\mathbf{x},\theta/\mathbf{y})e^{j\omega\tau}\, d\tau, \tag{A4}$$

where the autocorrelation function $C_{pp}(\mathbf{x},\theta/\mathbf{y})$ of the noise field radiated by a unit volume located at y is the axisymmetric version of the general expression given by Eq. (7). Using the various assumptions of the Ribner and Goldstein models, $I_\omega(\mathbf{x},\theta/\mathbf{y})$ may be expressed in terms of the statistical turbulent flow properties for the self- and shear noise.

Ribner model:

$$I_\omega^{\text{Se.N.}}(x,\theta/\mathbf{y})=\frac{\rho_0 L_1^3\overline{u_{tm}^2}^2}{128\pi^{5/2}c_0^5x^2}\frac{\omega^4}{\omega_f}\exp\left(-\frac{\omega^2C^2}{8\omega_f^2}\right)D_i^{\text{Se.N.}}, \tag{A5}$$

$$I_\omega^{\text{Sh.N}}(x,\theta/\mathbf{y})=\frac{\rho_0 L_1^5\overline{u_{tm}^2}}{24\pi^{7/2}c_0^5x^2}\left(\frac{\partial U_1}{\partial y_2}\right)^2\frac{\omega^4}{\omega_f}\times\exp\left(-\frac{\omega^2C^2}{4\omega_f^2}\right)D_i^{\text{Sh.N.}}. \tag{A6}$$

Goldstein model:

$$I_\omega^{\text{Se.N.}}(x,\theta/\mathbf{y})=\rho_0\frac{L_1L_2^2}{40\sqrt{2}\pi^{3/2}c_0^5x^2}\overline{u_{t1}^2}^2\frac{\omega^4}{\omega_f}\times\exp\left(-\frac{\omega^2C^2}{8\omega_f^2}\right)D_i^{\text{Se.N.}}, \tag{A7}$$

$$I_\omega^{\text{Sh.N.}}(x,\theta/\mathbf{y})=\rho_0\frac{L_1L_2^4\overline{u_{t1}^2}}{\pi^{3/2}c_0^5x^2}\left(\frac{\partial U_1}{\partial y_2}\right)^2\frac{\omega^4}{\omega_f}\times\exp\left(-\frac{\omega^2C^2}{4\omega_f^2}\right)D_i^{\text{Sh.N.}}, \tag{A8}$$

where the directivity for self- and shear noise in each model is given, respectively, in Secs. III B and C.

[1] M. J. Lighthill, "On sound generated aerodynamically—Part I. General theory," Proc. R. Soc. London Ser. A **211**, 564–587 (1952).

[2] M. J. Lighthill, "On sound generated aerodynamically—Part II. Turbulence as a source of sound," Proc. R. Soc. London Ser. A **222**, 1–32 (1954).

[3] I. Proudman, "The generation of sound by isotropic turbulence," Proc. R. Soc. London Ser. A **214**, 119–132 (1952).

[4] G. M. Lilley, "On the noise from air jets," Aeronaut. Res. Council ARC 20-376 (1958).

[5] H. S. Ribner, "The generation of sound by turbulent jets," in *Advances in Applied Mechanics* (Academic, New York, 1964).

[6] H. S. Ribner, "Quadrupole correlations governing the pattern of jet noise," J. Fluid Mech. **38**(1), 1–24 (1969).

[7] S. P. Pao and M. V. Lowson, "Some applications of jet noise theory," *8th Aerospace Sciences Meeting Conference* AIAA Paper 70-233 (New York, 1970).

[8] M. E. Goldstein and B. Rosenbaum, "Effect of anisotropic turbulence on aerodynamic noise," J. Acoust. Soc. Am. **54**, 630–645 (1973).

[9] A. J. Bilanin and J. E. Hirsh, "Application of second order turbulent modeling to the prediction of radiated aerodynamic sound," NASA-CR-2994 (1978).

[10] P. A. Lush, "Measurements of subsonic jet noise and comparison with theory," J. Fluid Mech. **46**(3), 477–500 (1971).

[11] D. Juve, J. Bataille, and G. Comte-Bellot, "Bruit de jets coaxiaux froids subsoniques," J. Méc. Appl. **2**(3), 385–398 (1978).

[12] J. E. Ffowcs Williams, "The noise from turbulence convected at high speed," Philos Trans. R. Soc. Sec. A **225**, 469–503 (1963).

[13] H. S. Ribner, "On spectra and directivity of jet noise," J. Acoust. Soc. Am. **35**, 614–616 (1963).

[14] W. Bechara, "Modélisation du bruit d'écoulements turbulents libres," Ecole Centrale Paris (France), 1992-02 (1992).

[15] P. O. A. L. Davies, M. J. Fisher, and M. J. Barratt, "The characteristics of the turbulence in the mixing region of a round jet," J. Fluid Mech. **15**(3), 337–367 (1963).

[16] M. L. Grant, "The large eddies of turbulent motion," J. Fluid Mech. **4**, 149 (1958).

[17] S. Chandrasekar, "The theory of axisymmetric turbulence," Philos. Trans. R. Soc. Ser. A **242**, 557–577 (1950).

[18] D. Laurence, "Code ULYSSE: Note de principe," Electricité De France—Direction des Etudes et Recherches (France, 1989).

[19] K. Chang and R. Lin, "A comparison of turbulence models for uses in calculations of free jets and flames," 27th Aerospace Sciences Meeting, Reno, Nevada, 1989.

[20] H. S. Pergament, N. Sinha, and S. M. Dash, "Hybrid two-equation turbulence model for high speed propulsive jets," *AIAA/ASME/SAE/ASEE 22nd Joint Propulsion Conference* (Huntsville, Alabama, 1986).

[21] D. D. Vandromme *et al.*, "Second order closure for the calculation of compressible wall bounded flows with an implicit Navier–Stokes Solver," Fourth Turbulent Shear Flows Conference, Karlsruhe, 1983.

[22] H. Ha Minh, *et al.* "On the use of second order modeling for the prediction of turbulent boundary layer/shok wave interactions: Physical and Numerical Aspects," Invited lectures of the international symposium on computational fluid dynamics, Tokyo, 1985.

[23] C. Berman, and J. Ramos, "Simultaneous computations of jet turbulence and noise," *12th Aeroacoustics Conference* (San Antonio, TX, 1989).

[24] A. M. Hecht, M. E. Teske, and A. J. Bilanin, "Predicting aerodynamic sound utilizing a two-point, two-time turbulence theory," *7th AIAA Aeroacoustics Conference* (Palto Alto, CA, 1981).

[25] D. G. Crighton, "Basic principles of aerodynamic noise generation," Prog. Aerospace Sci. **16**(1), 31–96 (1975).

[26] M. E. Goldstein, *Aeroacoustics* (McGraw-Hill, New York, 1976).

[27] M. Olsen and R. Friedman, "Jet noise from coaxial nozzles over a wide range of geometric and flow parameters," *12th Aerospace Sciences Meeting* AIAA Paper 74-43 (Washington, 1974).